REVISION IN THE MASS AND RADIUS OF KEPLER-11'S PLANETARY SYSTEM VIA PRECISE SPECTROSCOPIC CHARACTERIZATION

Megan Bedell[1], Jacob L. Bean[1], Jorge Meléndez[2], Sean Mills[1], Daniel C. Fabrycky[1], Ivan Ramírez[3], Martin Asplund[4], Fan Liu[4], David Yong[4]

Draft version August 19, 2016

ABSTRACT

The six planets of the Kepler-11 system are the archetypal example of a population of surprisingly low-density transiting planets revealed by the *Kepler* mission. We have determined the fundamental parameters and chemical composition of the Kepler-11 host star to unprecedented precision using an extremely high quality spectrum from Keck-HIRES (R≃67000, S/N≃260 at 600 nm). Contrary to previously published results, our spectroscopic constraints indicate that Kepler-11 is a young main-sequence solar twin. The revised stellar parameters raise the densities of the Kepler-11 planets by about 30%, making them more typical of the emerging class of "puffy" close-in exoplanets. We obtain photospheric abundances of 22 elements and find that Kepler-11 is enhanced in refractory materials relative to the solar abundance pattern. We additionally analyze the *Kepler* transits and transit timing variations (TTVs) using a photodynamical model and discuss the tension between spectroscopic and TTV-based stellar density estimates.

Subject headings: stars: abundances, stars: fundamental parameters, techniques: spectroscopic

1. INTRODUCTION

Five years after their initial discovery, the six planets of the Kepler-11 system remain a crown jewel of *Kepler* science results (Lissauer et al. 2011). All six planets orbit a Sun-like host star at low eccentricies in a largely co-planar, tightly packed configuration. The formation and long-term stability of the system remains an open question (see e.g. Ikoma & Hori 2012; Hands et al. 2014; Mahajan & Wu 2014). Kepler-11 is regarded as the proto-typical example of a "System with Tightly-packed Inner Planets" (STIP), a class of *Kepler* multi-planet systems which offer a surprising counterpoint to our own solar system's architecture. Given the low geometric probability of finding a six-planet transiting system, Kepler-11 is a valuable and rare opportunity to study in detail a common population of exoplanets.

In addition to their unusually tight system architecture, the Kepler-11 planets are noteworthy in another sense: their measured masses and radii place them among the lowest-density super-Earths known to date. Transit timing variations (TTVs) have been measured for all six planets. In the discovery paper, Lissauer et al. (2011, hereafter L11) derived mass constraints for the five inner planets based on TTVs from six quarters of *Kepler* data. Migaszewski et al. (2012) reanalyzed the same data using a photodynamical model and found similar results, with an additional constraint on the outermost planet mass. The system was later revisited by Lissauer et al.

(2013, hereafter L13) using fourteen quarters of *Kepler* data. All three analyses estimate mean densities of ≤ 0.5 $\rho_\oplus$ for all planets in the system, implying a considerable gas envelope on even the smaller super-Earths. This result has implications for potential formation scenarios, with the viability of forming such low-density planets on short orbits in situ up for debate (e.g. Lopez et al. 2012; Bodenheimer & Lissauer 2014; Howe & Burrows 2015).

Mean planet densities derived from transits and TTVs (or from transits and radial velocities) have a strong dependence on the assumed properties of the host star. Since the transit depth observationally constrains the ratio of planetary radius to stellar radius, the planet volume depends on the assumed stellar radius to the third power. The planet mass found from TTV inversion is correlated with the stellar mass. Host star characterization is therefore a critical part of measuring planet densities.

In past works, Kepler-11 has been characterized only through spectroscopic analysis of low to modest signal-to-noise data. Rowe et al. (L11, L13 2014) all use moderate signal-to-noise ratio spectra (S/N≤ 40) from Keck and apply the Spectroscopy Made Easy package (SME, Valenti & Piskunov 1996) to perform synthetic spectral matching. The resulting stellar atmospheric parameters, when compared with stellar evolution models, indicate that Kepler-11 is a slightly evolved solar analog with a density of 0.80 ± 0.04 $\rho_\odot$ (L13). No independent measurements of the stellar density (e.g. from astero-seismology or parallax) are available. Analysis of the stellar composition is also minimal. Adibekyan et al. (2012a) perform an equivalent width (EW) analysis on one of these Keck spectra to derive abundances of three α-elements and find that Kepler-11 has moderately low abundances of Ca, Cr, and Ti; however, the line list employed is quite limited with ≤ 5 lines per element.

Kepler-11's well-characterized planetary system makes it a prime target for more detailed spectroscopic study. In this work, we present an analysis of a new, very high

E-mail: mbedell@oddjob.uchicago.edu

[1] Department of Astronomy and Astrophysics, University of Chicago, 5640 S. Ellis Ave, Chicago, IL 60637, USA

[2] Departamento de Astronomia do IAG/USP, Universidade de São Paulo, Rua do Matão 1226, Cidade Universitária, 05508-900 São Paulo, SP, Brazil

[3] McDonald Observatory and Department of Astronomy, University of Texas at Austin, USA

[4] Research School of Astronomy and Astrophysics, The Australian National University, Cotter Road, Weston, ACT 2611, Australia

S/N spectrum. We use equivalent widths to measure the stellar properties and abundances of 22 elements at high precision.

The data are presented in Section 2. Derivation of the fundamental stellar properties from the spectrum is presented in Sections 3 and 4, and photospheric abundances are found in Section 5. We then present a new analysis of the *Kepler* lightcurve using a photodynamical model in Section 6. Finally, we compare the results from the spectroscopic and transit-based methods and discuss implications for the planetary system in Section 7.

2. DATA

Owing to its relative faintness (V = 14.2, L11), Kepler-11 was previously observed only at a signal-to-noise ratio insufficient for high-precision spectroscopic characterization. We dedicated nearly 8 hours of Keck I time to obtaining a higher quality spectrum. Over the course of two consecutive nights (July 26-27 2015), we made 22 1200-s exposures of Kepler-11 for a co-added result of S/N$\simeq$260 in the continuum near 600 nm. For these observations, HIRES was used with the B2 slit and kv387 filter, yielding a resolution R$\simeq$67000 and wavelength coverage between 390 and 830 nm.

We also observed the solar spectrum (via reflection from Ceres) and nine bright potential Kepler-11 twins with the same instrumental setup and similar S/N. The Kepler-11 twins were selected by imposing criteria of $5600 \leq T_{\rm eff} \leq 5750$ K and $4.2 \leq \log g \leq 4.4$ dex on databases of previously published stellar parameters (Adibekyan et al. 2012b; Bensby et al. 2014). Preference was given to stars likely to be thick-disk members with approximately solar metallicity. These criteria were set based on the original spectroscopic analysis of Kepler-11 by L11, who found $T_{\rm eff} = 5680 \pm 100$ K, $\log g = 4.3 \pm 0.2$ dex, [Fe/H]= 0.0 ± 0.1 dex, and a significant chance of Kepler-11's being a thick disk member based on its kinematics.

The spectral extraction was performed by the Mauna Kea Echelle Extraction (MAKEE) pipeline. All Kepler-11 spectra were then co-added using IRAF's *scombine*.[5] Continuum normalization was done by fitting low-order polynomial functions to each order, with care to use the same functional order for a given spectral order on every stellar spectrum to avoid bias in the subsequent differential analysis. Doppler corrections were applied using IRAF's *dopcor* task.

3. STELLAR PROPERTIES FROM SPECTROSCOPIC ANALYSIS

The fundamental properties of Kepler-11 and its potential twins were derived from an equivalent width analysis. We hand-measured 94 Fe I and 17 Fe II spectral lines using IRAF's *splot*. The line list used unblended and unsaturated iron lines adapted from previous works such as Ramírez et al. (2014). Laboratory values for transition probability where adopted where available, but for this strictly differential analysis the values of $\log gf$ and χ are largely irrelevant, since they cancel out for all lines in the linear region of the curve-of-growth. Equivalent widths

were measured by carefully choosing local continua as described in Bedell et al. (2014) to maximize differential precision between the spectra. The full line list and measured equivalent widths are available in Table 3.

The stellar effective temperature $T_{\rm eff}$, surface gravity $\log g$, metallicity [M/H], and microturbulence v_t were determined by imposing a set of requirements on the iron abundances derived by MOOG (Sneden 1973). Namely, we required the [Fe/H] abundances from both ionization states to be equal, and any trends in iron abundance with the excitation potential or reduced equivalent width of the lines to be minimized. As the most readily observable abundant metal in the photosphere, we used iron abundance [Fe/H] as a direct proxy for metallicity [M/H]. It is important to note that we exclusively used the *differential* abundance measurements relative to the solar spectrum for this analysis. By directly comparing line-by-line differential abundances of spectrally similar stars, we minimize the influence of stellar model systematics on the final parameters and abundances (see e.g. Ramírez et al. 2014).

Parameter solutions were found iteratively using the q^2 python package.[6] Uncertainties were determined by propagating scatter among the measured line abundances as described in Epstein et al. (2010); Bensby et al. (2014).

The resulting stellar parameters for all observed stars are given in Table 1. The $T_{\rm eff}$ and $\log g$ for Kepler-11 are significantly higher than previously determined values. We find $T_{\rm eff} = 5839 \pm 7$ K, $\log g = 4.45 \pm 0.02$ dex, and [Fe/H]= 0.06 ± 0.01 dex, while L13, for example, find $T_{\rm eff} = 5666 \pm 60$ K, $\log g = 4.28 \pm 0.07$ dex, and [Fe/H]= 0.00 ± 0.04 dex. Potential sources of this tension include the substantially different S/N of spectra used and the difference in analysis technique. L13 and other previous analyses use SME, which employs synthetic spectra to do spectral matching. (systemic error or just underestimated errors? check literature)

Our revised stellar parameters securely place Kepler-11 in the solar twin category. This can be seen even by eye: as depicted in Figure 1, at high S/N Kepler-11's spectrum is nearly identical to the solar spectrum and distinctly different from that of HD1178, the star from our sample whose fundamental parameters most closely match those found by L13. In particular, the solar-like $\log g$ for Kepler-11 implies that it is denser and less evolved than previously thought.

We used stellar evolutionary models to estimate the mass, radius, and age of Kepler-11. Yonsei-Yale isochrones were fit using q^2 (Figure 2). We also applied Dartmouth and Basti isochrones using the *isochrones* python package for fitting (Morton 2015). All three models gave results consistent within well below 1σ. From these fits, we estimate a stellar mass $M_\star = 1.04 \pm 0.01$ $M_\odot$, radius $R_\star = 1.00 \pm 0.02$ $R_\odot$, and age 2.8 ± 0.8 Gyr. This gives a stellar density $\rho_\star = 1.47 \pm 0.09$ g cm^{-3}.

4. ALTERNATIVE STELLAR AGE INDICATORS

While mass, radius, and density cannot be measured through methods other than the stellar spectrum, stellar age has multiple known proxies. We used several alternate methods to measure the age of Kepler-11 as an independent test of its evolutionary state. The results

---

[5]IRAF is distributed by the National Optical Astronomy Observatory, which is operated by the Association of Universities for Research in Astronomy (AURA) under cooperative agreement with the National Science Foundation.

[6]https://github.com/astroChasqui/q2

TABLE 1
Summary of derived fundamental stellar properties.

| Spectrum	$T_{\rm eff}$ (K)	σ_T (K)	$\log g$ (dex)	σ_{logg} (dex)	v_t (km s^{-1})	σ_{v_t} (km s^{-1})	[Fe/H] (dex)	$\sigma_{[Fe/H]}$ (dex)
Sun (Ceres) [a]	5777	–	4.44	–	0.97	–	0.0	–
K11	5840	7	4.46	0.02	1.00	0.02	0.063	0.007
HD1178	5644	10	4.34	0.03	0.89	0.03	0.013	0.010
HD10145	5627	20	4.33	0.05	0.81	0.06	-0.017	0.021
HD16623	5833	47	4.51	0.09	1.07	0.10	-0.434	0.034
HD20329	5592	16	4.32	0.04	0.80	0.05	-0.094	0.015
HD21727	5608	21	4.32	0.06	0.82	0.07	0.010	0.020
HD21774	5757	27	4.33	0.06	0.99	0.06	0.251	0.024
HD28474	5808	43	4.60	0.08	1.06	0.10	-0.578	0.030
HD176733	5597	15	4.33	0.04	0.77	0.05	-0.012	0.014
HD191069	5739	29	4.33	0.09	1.03	0.08	-0.029	0.025

[a]Used as reference star.
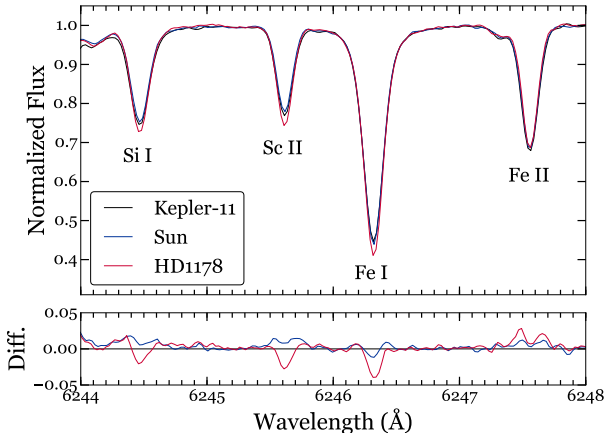
Fig. 1.— A small section of the Keck-HIRES spectra of the Sun (blue), Kepler-11 (black), and HD1178 (red), which has fundamental parameters similar to those given by Lissauer et al. (2013) for Kepler-11. Residuals for flux relative to the Kepler-11 spectrum are plotted in the lower panel.
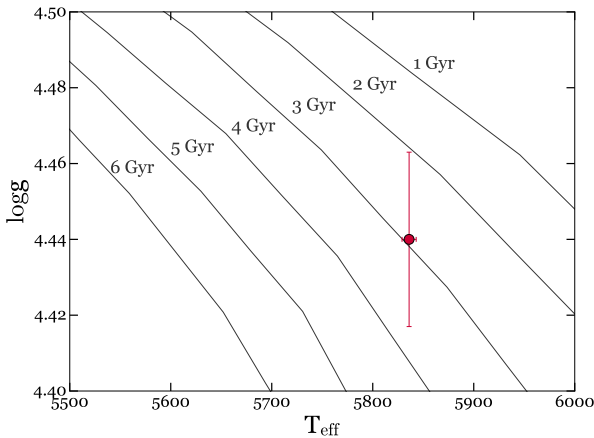

Fig. 2.— Measured stellar properties of Kepler-11 plotted with Yonsei-Yale isochrones at a metallicity of 0.06 dex.

unanimously agree upon a sub-solar age for Kepler-11 (table?). Details of the methods used follow.

4.1. Stellar Rotation

The apparent rotation rate $v \sin i$ was measured using five saturated lines (Fe I 6027.050 Å, 6151.618 Å, 6165.360 Å, 6705.102 Å, and Ni I 6767.772 Å) from the Keck spectrum. The procedure used is described in depth in dos Santos et al. (2016), and will be summarized here. We first measured the macroturbulence value $v_{\rm macro,\odot}$ for each line in the solar reference spectrum using MOOG *synth* with $v \sin i_\odot$ fixed at 1.9 km s^{-1}. We then calculated $v_{\rm macro}$ for Kepler-11 using the measured solar values and the empirical relation given in Equation 1 of dos Santos et al. (2016). Finally, MOOG *synth* was used to find $v \sin i$ for each line in Kepler-11's spectrum with $v_{\rm macro}$ fixed to the calculated value.

The five lines give a consistent result of $v \sin i = 2.2 \pm 0.2$ km s^{-1}. Assuming alignment of the stellar spin axis with the orbital axis of its transiting planets, we can take $v \sin i$ as the true rotational velocity. (starspots in LC?) This translates to an age of 3.4 Gyr using the law of Skumanich (1972) anchored by the Sun, or 3.0 ± 2.9?? Gyr from dos Santos et al. (2016)'s updated relation.

4.2. Lithium Abundance

The lithium abundance of Kepler-11 was measured by synthesizing the Li I 6707.8 Å line with MOOG *synth*. The line list was adopted from Meléndez et al. (2012) and includes blends of atomic and molecular lines. We find a lithium abundance of $A(\rm Li) = 1.26 \pm 0.05$, higher than the solar value of 1.11 at the level of 3σ (Figure 3). This implies a sub-solar age, since lithium is steadily depleted throughout a star's main-sequence lifetime (cite).

4.3. [Y/Mg] Abundance Ratio

Recent works by Nissen (2015) and Tucci Maia et al. (2016) have identified the ratio of yttrium to magnesium abundances as an excellent proxy for age in main-sequence Sun-like stars. We measured these abundances as described in Section 5 and found a [Y/Mg] ratio of 0.04 $\pm$ 0.05 dex. Using the age relation from Tucci Maia et al. (2016), this gives an age of 4.0 ± 0.7 Gyr. double-check these numbers

4.4. Chromospheric Emission

We measured the chromospheric emission level of Kepler-11 using the Ca II H line. Since our spectral coverage cut off around 390 nm at the blue end, it was not possible to obtain a measurement of the standard chromospheric activity index $\log(\rm R'_{HK})$. Instead, we defined
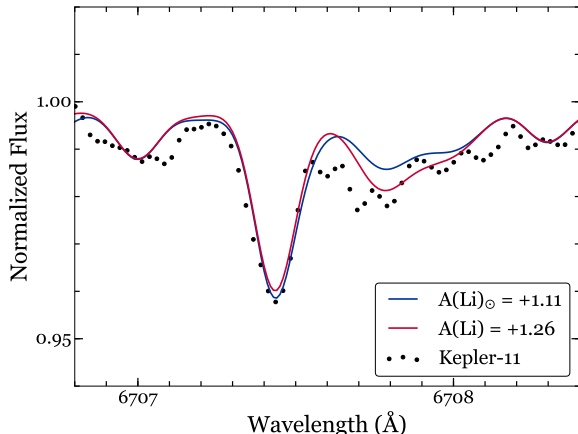
FIG. 3.— Observed spectrum of Kepler-11 around the Li I 6707.8 Å line. Synthetic fits for the best-fit Li abundance (red) and the solar Li abundance (blue) are overplotted. (fix up this fit!)

an alternative index H as the flux integrated from a 1.3 Å width triangular filter centered on the H line at 3968.47 Å, divided by the continuum integrated with a flat filter of 5 Å width around 3979.8 Å. conversion details

We find an activity index $\log(R'_{HK})$ = -4.78. This is slightly higher than the maximum activity level of the solar cycle and suggests a sub-solar age (Hall et al. 2009; Ramírez et al. 2014).

5. STELLAR ABUNDANCES

We measured photospheric abundances using the curve-of-growth technique for 20 other elements (excluding lithium, whose synthesis-based abundance determination is discussed in Section 4.2). As with the iron lines, all equivalent widths were measured by hand and line-by-line differential abundances determined with MOOG using q^2. The line list was adapted from previous works including Bedell et al. (2014). Hyperfine structure corrections were applied for Co I, Cu I, Mn I, V I, and Y II following (cite). Carbon abundances were measured by a combination of C I and CH lines. Errors on the final abundances were found by adding in quadrature the intrinsic scatter of the lines and the uncertainty propagated from errors on the stellar parameters. The measured equivalent widths are given in Table 3, and resulting abundances for all stars are in Table 4.

Kepler-11's status as a solar twin enables direct comparison of its abundance pattern to that of the Sun and other known solar twins. Of particular interest is the question of trends in elemental abundances with condensation temperature (T_C). As shown by Meléndez et al. (2009), the solar abundance pattern is unusual in its depletion of refractory elements relative to volatiles. This depletion has been interpreted as "missing" rocky material that is locked up in the Solar System planets (Chambers 2010). Building up the number of stars with precisely characterized abundance patterns and planetary systems can help to test this possibility.

We apply corrections for the effects of galactic chemical evolution (GCE), which can change the abundance patterns and T_C trends of stars at varying ages (Nissen 2015; Spina et al. 2016b). We correct each abundance [X/H] using the prescription of Spina et al. (2016a), who fit hy-perbolic relations to [X/H] as a function of stellar age for a sample of solar twins. We then use the corrected abundances and T_C values from Table 8 of Lodders (2003) to search for a trend. For this part of the analysis, all measured states of a given element (e.g. CI and CH, TiI and TiII, etc.) were combined with a weighted average for the overall elemental abundance.

Based on our analysis, Kepler-11 appears to be a "typical" solar twin: that is, its abundance pattern is enhanced in refractories relative to the solar pattern (Figure 4). The significance of this enhancement depends on the stellar age adopted for the GCE correction. Without GCE correction applied, the T_C slope is significant only at the 2σ level, whereas adopting an age of 2.8 Gyr enhances the slope to above 3σ.

(Adjust Tc figure & discussion to use bootstrapped errors on slope.)

6. STELLAR PROPERTIES FROM PHOTODYNAMIC TRANSIT ANALYSIS

In order to reassess the stellar density constraint based on the transit data, we performed a photodynamical fit to the full *Kepler* short cadence (58.8 second exposure) data set. The model integrates the 7-body Newtonian equations of motions for the central star and two planets, including the light–travel–time effect. When the planets pass between the star and the line of sight, a synthetic light curve is generated (Pál 2012), which can then be compared to the data. This approach therefore takes into account all transit-timing variations and can constrain planet masses and eccentricities as well as radii. To prepare the data for fitting, we detrended the data with a cubic polynomial with a 2880 minute (2 day) width every 100 points, and interpolated for points between. We divide the flux by this fit as a baseline to generate our data set of 1746779 points. We additionally multiply the uncertainties given by *Kepler* by a factor of 1.115318 so that the reduced χ^2 of a fiducial model was 1.0. This will broaden our posteriors and helps take into account unmodeled noise in the data. To simultaneously generate the posteriors on all of our model parameters, we ran differential evolution Markov chain Monte Carlo (DEM-CMC, Ter Braak 2005) fits with planetary parameters $\{P, T_0, e^{1/2}\cos(\omega), e^{1/2}\sin(\omega), i, \Omega, R_p/R_\star, M_p/M_\star\}$ for all planets, where P is the period, T_0 is the mid-transit time, e is eccentricity, ω is the argument of periapse, i is inclination, Ω is nodal angle, and R and M are radius and mass respectively (with subscripts p = b, c, d, e, f, g for the planets and $\star$ for the star). The star had five additional parameters: $\{M_\star, R_\star, c_1, c_2, dilute\}$, where $\{c_i\}$ are the two quadratic limb-darkening coefficients and $dilute$ is the amount of dilution from other nearby sources. We use eccentricity vector components scaling as $e^{1/2}$ so that we have flat prior in total e, and fix the values of $dilute = 0$ since there is no evidence of other nearby stars diluting the lightcurve. We also fix the value of $M_\star$ as transits alone generally only give information about the density of the star, rather than $M_\star$ and $R_\star$ individually. We fix $\Omega = 0$ for all planets because the data is not precise enough to constrain these values (Migaszewski et al. 2012). Additionally, it is extremely unlikely that there are large mutual inclinations among the planets given that we see six planets transit (L11,
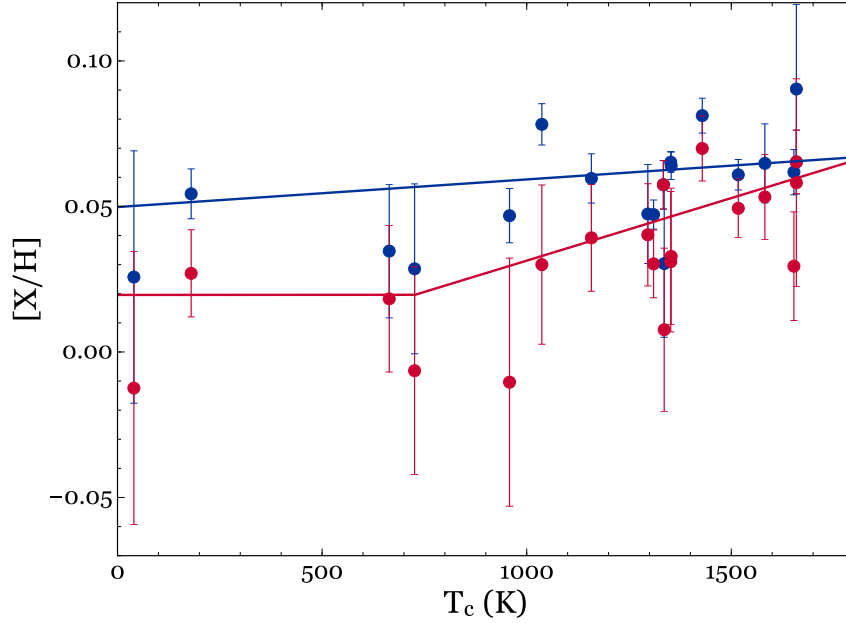
FIG. 4.— Differential element abundances of Kepler-11 as a function of the condensation temperature of the element within the protoplanetary disk. The spectral abundances are plotted in blue, and abundances after a GCE correction is applied are in red. Note that the uncertainties increase after GCE correction due to the propagated uncertainty in the correction factors and in the stellar age. Best-fit models were derived using a least-squares fit to a linear piecewise function with the temperature break as a free parameter. (add in a legend with slope values and errors)

Figure 4), five of which are dynamically packed and thus have no misaligned non-transiting planets between them (L11). We use flat priors in all other parameters.

We run two DEMCMCs. One has no constraints on the stellar radius, i.e., allows the transits themselves to completely determine the stellar density, which we will label $\mathcal{NSI}$, for No Spectral Information. The second DEMCMC we run with the stellar mass and radius fixed at the spectroscopically measured values in this study, $M_\star = 1.04 M_\odot$ and $R_\star = 1.00 M_\odot$, which we will label $\mathcal{FSP}$, for Fixed Stellar Parameters. The $\mathcal{NSI}$ run produces a lower density star $\rho_\star = 1.191^{+0.043}_{-0.11}$ g cm^{-3} than the fixed value of $\rho_\star = 1.466$ g cm^{-3} in $\mathcal{FSP}$. This indicates that the transit data alone are discrepant with the spectroscopically measured stellar density. Table 2 shows the density results for all bodies for both DEMCMC runs. We note that the densities of planets with no spectral information, $\mathcal{NSI}$, are slightly higher than reported in L13 because that study includes the lower spectroscopically measured stellar density in their final best fits.

The best fit solution from $\mathcal{NSI}$ run has $\chi^2 = 1746731$, while the $\mathcal{FSP}$ run has $\chi^2 = 1746778$, a difference of 47. Thus we see that fixing the stellar parameters at their spectroscopically measured values causes the fit to the *Kepler* data to become statistically significantly worse since there is only one more degree of freedom (stellar density) in the $\mathcal{NSI}$ model than the $\mathcal{FSP}$ model. This confirms the existence of tension between the transit measured stellar density and the spectroscopically measured one.

7. DISCUSSION

7.1. *Discrepancies in Stellar Densities*

TABLE 2
STAR AND PLANET DENSITIES

Body	$\mathcal{NSI}$	$\mathcal{FSP}$
	Density (g cm^{-3})	Density (g cm^{-3})
Kepler-11	$1.191^{+0.043}_{-0.11}$	1.466 (fixed)
Kepler-11 b	$2.43^{+0.64}_{-0.61}$	$3.14^{+0.71}_{-0.76}$
Kepler-11 c	$1.09^{+0.31}_{-0.31}$	$1.41^{+0.35}_{-0.40}$
Kepler-11 d	$1.32^{+0.14}_{-0.15}$	$1.53^{+0.13}_{-0.14}$
Kepler-11 e	$0.657^{+0.076}_{-0.080}$	$0.749^{+0.092}_{-0.093}$
Kepler-11 f	$0.82^{+0.17}_{-0.15}$	$0.67^{+0.24}_{-0.23}$
Kepler-11 g	< 4	< 5

NOTE. — Medians and 1-σ uncertainties from the DEMCMC runs as described in § 6
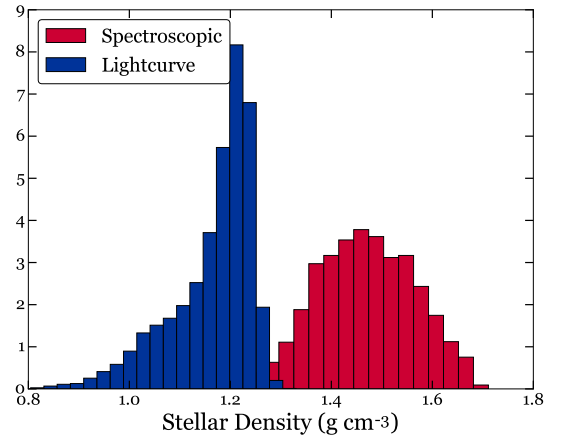

FIG. 5.— Posterior distributions for the stellar density from isochrone fits to the spectroscopic parameters (red) and from photodynamical modeling of the lightcurve (blue).

The stellar densities found through spectroscopic characterization (1.47 ± 0.09 g cm^{-3}) and photodynamical modeling (1.13 ± 0.07 g cm^{-3}) are inconsistent at the level of $\sim 3\sigma$ (is this true anymore? why did it change?) (Figure 5). While spectroscopically-derived densities can be strongly dependent on imperfect stellar isochrone models, we note that in this case Kepler-11's extreme similarity to the Sun places it near the anchor point of most models, increasing the accuracy of isochronal analysis. Moreover, multiple independent methods support the result of a young, non-evolved age and therefore a solar-like density for Kepler-11.

An alternative hypothesis is that some bias in the transit analysis has resulted in an erroneously low inferred stellar density. As described by Kipping (2014), multiple effects can bias the density measured by transits, including stellar activity, blended background sources, and non-zero planet eccentricities. Bias due to an underestimated planet eccentricity is not a likely explanation in this case, since all five planets give a consistent stellar density. Also, the photodynamical modeling used in this analysis should be robust to the effects of transit timing or duration variations on the measured stellar density. This leaves two potentially viable explanations from Kipping (2014) for the density discrepancy: stellar activity (the "photospot" effect) or a background source (the "photoblend" effect).

Starspots effectively reduce the observed stellar flux, artificially raising stellar density inferred from the transit depth, which is the opposite of the effect we seek to explain. However, as a middle-aged Sun-like star, Kepler-11's activity may manifest mostly in the form of plages (cite). Unocculted plages could potentially lower the observed stellar density. Given the observed behavior of other main-sequence solar analogs and the lack of rotational modulation in the *Kepler* lightcurve, the filling factor for spots or plages on Kepler-11's surface should be of order 1% (cite). This would yield a similarly small change in the observed stellar density ($O(10^{-2})$, Kipping 2014). Furthermore, the plage configuration would need to be relatively stable throughout *Kepler* 's four years of observations, since the transit depths do not noticeably change with time (check with Sean on this), which is unlikely at the high level of activity needed to have a filling factor $\gg 1\%$.

The final effect is blending of unresolved background sources, which can cause stellar density to be underestimated. Recently Wang et al. (2015) found two visual companions to Kepler-11 at separations of 1.36" and 4.9" using AO imaging, both potentially within Kepler's resolution. With brightness differences of $\Delta K = 4.4$ mag and 4.7 mag respectively, these companions should contribute approximately 3% of the total flux in the Kepler bandpass (true?). Using Equation 9 of Kipping (2014), this implies that the observed stellar density from transits should be $\sim 99\%$ of the true density. The known

companions are therefore insufficient to explain the magnitude of the density discrepancy.
so....?

7.2. *Implications for the Planets*

The mass and radius of Kepler-11 has considerable repercussions for its planetary system. We approximate the planet mass derived from TTVs as a linear function of the assumed stellar mass. The planet radius also has a linear dependence on stellar radius, since only the relative surface areas of planet and star can be measured by the transit depth. The stellar properties obtained through spectroscopic analysis therefore raise the planet masses by a factor of 8% and lower the planet radii by a factor of 6% relative to the transit and TTV-derived values. The results are shown in Figure 6.

Adopting the stellar properties from spectroscopic analysis raises the mean densities of the Kepler-11 planets by $\sim 30\%$. This change may go a long way in resolving the lingering debate over the viability of in-situ formation of these planets. (finish - talk to Leslie?)

7.3. *Stellar Composition & Planets*
compare to Kepler-10, Sun

8. CONCLUSION

Using an extremely high-quality spectrum of the multi-planet host star Kepler-11, we have measured the stellar fundamental parameters and abundances to percent-level precision. We have also used a photodynamical model to fit the full *Kepler* lightcurve. Our planet parameters agree with past publications. However, we find that the host star is younger than previously thought by a factor of ~ 3. Based on spectroscopic results, Kepler-11 and its planets are $\sim 30\%$ denser than previously reported.

The five inner planets of the Kepler-11 system are key members of the exoplanet mass-radius diagram as examples of the surprisingly low densities found in some planetary systems. The substantial revision of their properties reported here underscores the importance of detailed host star follow-up. As the community looks to exponentially increase the number of exoplanets with measured bulk densities through TESS and beyond, it is critical to prioritize securing high-quality spectra of the host stars to enable the determination of precise host star properties.

Facilities: Keck:I (HIRES), Kepler

REFERENCES

Adibekyan, V. Z., Delgado Mena, E., Sousa, S. G., et al. 2012a, A&A, 547, A36

Adibekyan, V. Z., Sousa, S. G., Santos, N. C., et al. 2012b, A&A, 545, A32

Bedell, M., Meléndez, J., Bean, J. L., et al. 2014, ApJ, 795, 23

Bensby, T., Feltzing, S., & Oey, M. S. 2014, A&A, 562, A71

Bodenheimer, P., & Lissauer, J. J. 2014, ApJ, 791, 103

Chambers, J. E. 2010, ApJ, 724, 92

dos Santos, L. A., Meléndez, J., do Nascimento, Jr., J.-D., et al. 2016, A&A, arXiv:1606.06214

Epstein, C. R., Johnson, J. a., Dong, S., et al. 2010, The Astrophysical Journal, 709, 447
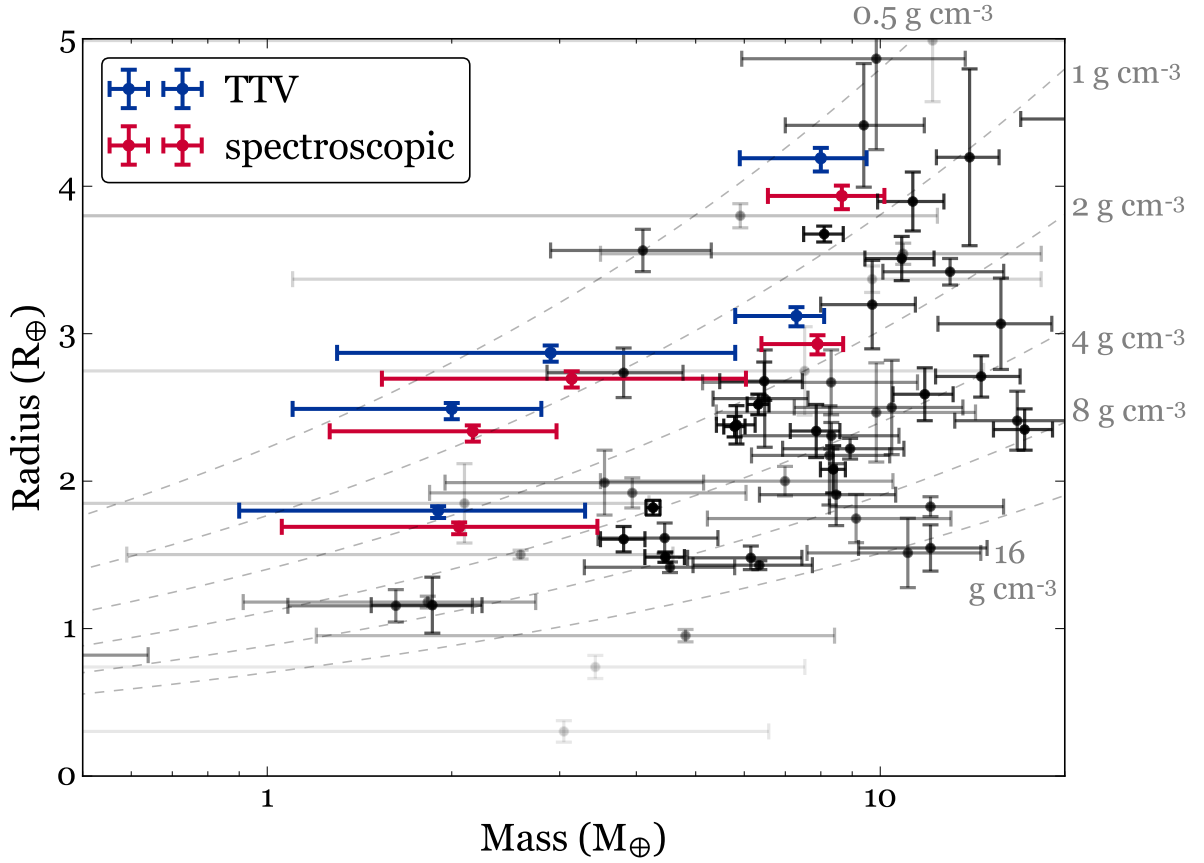
FIG. 6.— Exoplanets with measured masses and radii. Transparencies of the black points scale with the relative error on planet parameters. Kepler-11 a-e are plotted in red (using the transit and TTV-derived parameters) and blue (adjusted by the spectroscopic stellar parameters). Dashed lines show fixed mean densities.

Hall, J. C., Henry, G. W., Lockwood, G. W., Skiff, B. A., & Saar, S. H. 2009, AJ, 138, 312
Hands, T. O., Alexander, R. D., & Dehnen, W. 2014, MNRAS, 445, 749
Howe, A. R., & Burrows, A. 2015, ApJ, 808, 150
Ikoma, M., & Hori, Y. 2012, ApJ, 753, 66
Kipping, D. M. 2014, MNRAS, 440, 2164
Lissauer, J. J., Fabrycky, D. C., Ford, E. B., et al. 2011, Nature, 470, 53
Lissauer, J. J., Jontof-Hutter, D., Rowe, J. F., et al. 2013, ApJ, 770, 131
Lodders, K. 2003, ApJ, 591, 1220
Lopez, E. D., Fortney, J. J., & Miller, N. 2012, ApJ, 761, 59
Mahajan, N., & Wu, Y. 2014, ApJ, 795, 32
Meléndez, J., Asplund, M., Gustafsson, B., & Yong, D. 2009, ApJ, 704, L66
Meléndez, J., Bergemann, M., Cohen, J. G., et al. 2012, A&A, 543, A29
Migaszewski, C., Słonina, M., & Goździewski, K. 2012, MNRAS, 427, 770

Morton, T. D. 2015, isochrones: Stellar model grid package, Astrophysics Source Code Library, ascl:1503.010
Nissen, P. E. 2015, A&A, 579, A52
Pál, A. 2012, MNRAS, 420, 1630
Ramírez, I., Meléndez, J., Bean, J., et al. 2014, A&A, 572, A48
Rowe, J. F., Bryson, S. T., Marcy, G. W., et al. 2014, ApJ, 784, 45
Skumanich, A. 1972, ApJ, 171, 565
Sneden, C. A. 1973, PhD thesis, THE UNIVERSITY OF TEXAS AT AUSTIN.
Spina, L., Meléndez, J., Karakas, A. I., et al. 2016a, A&A
Spina, L., Meléndez, J., & Ramírez, I. 2016b, A&A, 585, A152
Ter Braak, C. J. F. 2005, Wageningen UR, Biometris, 010404, 556
Tucci Maia, M., Ramírez, I., Meléndez, J., et al. 2016, A&A, 590, A32
Valenti, J. A., & Piskunov, N. 1996, A&AS, 118, 595
Wang, J., Fischer, D. A., Horch, E. P., & Xie, J.-W. 2015, ApJ, 806, 248

TABLE 3
LINE LIST AND MEASURED EQUIVALENT WIDTHS.

Wavelength (Å)	Species	EP (eV)	log(gf) (dex)	Kepler-11 (mÅ)	Sun (mÅ)	HD1178 (mÅ)	HD10145 (mÅ)	HD16623 (mÅ)	HD20329 (mÅ)	HD21727 (mÅ)	HD21774 (mÅ)	HD28474 (mÅ)	HD176733 (mÅ)	HD191069 (mÅ)
5052.167	6	7.685	-1.24	35.2	33.5	32.7	27.9	21.4	29.4	26.6	41.6	17	27.4	36.7
6587.61	6	8.537	-1.05	16.9	15.2	17	12.2	9.8	11.4	11.7	20.3	6.2	10.8	17
7111.47	6	8.64	-1.07	13.2	11.3	12.1	15.1	9.6	12.3	10.9	16.6	36.7	10.2	14
7113.179	6	8.647	-0.76	25.3	22.4	23.2	20.3	13.8	17.9	19.5	33	11.3	18.2	24.3
7771.944	8	9.146	0.37	77.8	69.7	79.1	63.6	71	69.4	62.9	79.9	56.9	61.5	81.8
								...						

NOTE. — Table 3 is published in its entirety in the electronic edition of ApJ. A portion is shown here for guidance regarding its form and content.

TABLE 4
DIFFERENTIAL ABUNDANCES [X/H].

Element	N_{lines}	Kepler-11	HD1178	HD10145	HD16623	HD20329	HD21727	HD21774	HD28474	HD176733	HD191069
CI	4	0.03 ± 0.01	0.12 ± 0.04	0.06 ± 0.12	-0.19 ± 0.08	0.05 ± 0.08	0.02 ± 0.06	0.18 ± 0.04	-0.07 ± 0.45	-0.00 ± 0.05	0.07 ± 0.03
OI	3	0.05 ± 0.01	0.18 ± 0.08	0.08 ± 0.02	-0.08 ± 0.02	0.18 ± 0.03	0.07 ± 0.03	0.20 ± 0.02	-0.25 ± 0.02	0.05 ± 0.03	0.14 ± 0.02
NaI	4	0.05 ± 0.02	-0.03 ± 0.02	-0.12 ± 0.05	-0.37 ± 0.02	-0.04 ± 0.04	-0.08 ± 0.03	0.27 ± 0.03	-0.54 ± 0.05	-0.03 ± 0.03	-0.01 ± 0.02
MgI	5	0.03 ± 0.05	0.39 ± 0.48	0.34 ± 0.48	-0.07 ± 0.55	0.12 ± 0.20	0.35 ± 0.47	0.36 ± 0.16	-0.27 ± 0.54	0.32 ± 0.48	0.35 ± 0.49
AlI	2	0.06 ± 0.01	0.18 ± 0.02	0.03 ± 0.00	-0.28 ± 0.01	0.18 ± 0.02	0.08 ± 0.00	0.28 ± 0.01	-0.45 ± 0.01	0.04 ± 0.00	0.11 ± 0.01
SiI	14	0.05 ± 0.02	0.04 ± 0.03	-0.00 ± 0.01	-0.27 ± 0.03	0.04 ± 0.05	0.02 ± 0.03	0.25 ± 0.02	-0.44 ± 0.04	-0.01 ± 0.02	0.04 ± 0.01
SI	4	0.04 ± 0.04	0.10 ± 0.04	0.05 ± 0.03	-0.23 ± 0.06	0.03 ± 0.09	0.01 ± 0.03	0.24 ± 0.03	-0.36 ± 0.09	0.02 ± 0.05	0.09 ± 0.05
KI	1	0.07 ± 0.00	0.07 ± 0.00	0.02 ± 0.00	-0.22 ± 0.00	0.03 ± 0.00	0.01 ± 0.00	0.15 ± 0.00	-0.42 ± 0.00	-0.00 ± 0.00	0.08 ± 0.00
CaI	11	0.06 ± 0.02	0.02 ± 0.14	-0.05 ± 0.17	-0.28 ± 0.05	0.18 ± 0.24	0.04 ± 0.15	0.19 ± 0.08	-0.47 ± 0.06	-0.07 ± 0.20	0.04 ± 0.03
ScI	4	0.09 ± 0.04	0.09 ± 0.03	0.02 ± 0.03	-0.30 ± 0.06	0.06 ± 0.06	0.03 ± 0.03	0.27 ± 0.03	-0.33 ± 0.08	-0.01 ± 0.04	0.08 ± 0.01
ScII	5	0.09 ± 0.02	0.14 ± 0.06	0.03 ± 0.02	-0.24 ± 0.04	0.14 ± 0.06	0.10 ± 0.05	0.32 ± 0.02	-0.41 ± 0.05	-0.00 ± 0.02	0.12 ± 0.04
TiI	18	0.07 ± 0.02	0.12 ± 0.03	0.05 ± 0.05	-0.21 ± 0.04	0.15 ± 0.03	0.07 ± 0.04	0.24 ± 0.04	-0.41 ± 0.03	0.02 ± 0.03	0.08 ± 0.02
TiII	11	0.07 ± 0.03	0.11 ± 0.05	0.01 ± 0.09	-0.18 ± 0.05	0.11 ± 0.03	0.01 ± 0.10	0.26 ± 0.04	-0.37 ± 0.04	-0.02 ± 0.03	0.11 ± 0.04
VI	9	0.08 ± 0.02	0.07 ± 0.02	-0.02 ± 0.03	-0.28 ± 0.03	0.08 ± 0.09	0.04 ± 0.03	0.28 ± 0.02	-0.48 ± 0.04	-0.00 ± 0.02	0.04 ± 0.02
CrI	10	0.04 ± 0.02	0.02 ± 0.03	0.01 ± 0.07	-0.47 ± 0.03	-0.06 ± 0.03	0.02 ± 0.03	0.27 ± 0.03	-0.60 ± 0.06	0.01 ± 0.03	-0.02 ± 0.02
CrII	5	0.05 ± 0.02	0.01 ± 0.02	-0.02 ± 0.05	-0.38 ± 0.06	-0.08 ± 0.02	0.01 ± 0.03	0.24 ± 0.03	-0.55 ± 0.05	-0.03 ± 0.04	-0.02 ± 0.02
MnI	8	0.06 ± 0.02	-0.04 ± 0.03	-0.07 ± 0.04	-0.61 ± 0.02	-0.18 ± 0.02	-0.04 ± 0.03	0.30 ± 0.03	-0.75 ± 0.06	-0.02 ± 0.03	-0.08 ± 0.02
FeI	92	0.06 ± 0.03	0.02 ± 0.04	-0.02 ± 0.06	-0.43 ± 0.09	-0.09 ± 0.05	0.01 ± 0.08	0.25 ± 0.08	-0.58 ± 0.08	-0.01 ± 0.05	-0.03 ± 0.09
FeII	17	0.06 ± 0.02	0.02 ± 0.05	-0.02 ± 0.11	-0.43 ± 0.07	-0.10 ± 0.05	0.00 ± 0.04	0.25 ± 0.03	-0.58 ± 0.07	-0.02 ± 0.03	-0.03 ± 0.04
CoI	6	0.07 ± 0.01	0.05 ± 0.04	-0.04 ± 0.03	-0.27 ± 0.04	0.01 ± 0.03	-0.01 ± 0.03	0.26 ± 0.01	-0.45 ± 0.03	-0.02 ± 0.01	0.06 ± 0.02
NiI	20	0.06 ± 0.02	0.00 ± 0.07	-0.03 ± 0.03	-0.42 ± 0.03	-0.05 ± 0.04	0.01 ± 0.05	0.31 ± 0.16	-0.60 ± 0.03	0.00 ± 0.05	-0.01 ± 0.02
CuI	4	0.08 ± 0.01	0.08 ± 0.03	-0.02 ± 0.02	-0.44 ± 0.05	0.00 ± 0.01	-0.00 ± 0.02	0.32 ± 0.03	-0.59 ± 0.09	0.06 ± 0.03	0.06 ± 0.02
ZnI	3	0.03 ± 0.04	0.05 ± 0.02	0.01 ± 0.04	-0.31 ± 0.06	0.07 ± 0.02	-0.00 ± 0.03	0.28 ± 0.05	-0.52 ± 0.09	0.00 ± 0.02	0.08 ± 0.02
YII	5	0.07 ± 0.02	-0.01 ± 0.01	-0.05 ± 0.03	-0.52 ± 0.03	-0.12 ± 0.03	-0.04 ± 0.02	0.23 ± 0.01	-0.61 ± 0.04	-0.04 ± 0.03	-0.08 ± 0.01
CH	3	0.03 ± 0.05	0.03 ± 0.12	-0.04 ± 0.13	-0.45 ± 0.11	-0.17 ± 0.09	-0.05 ± 0.09	0.24 ± 0.05	-0.65 ± 0.14	-0.08 ± 0.29	0.04 ± 0.08